IEEE Access
Multidisciplinary | Rapid Review | Open Access Journal

Received 23 July 2022, accepted 15 August 2022, date of publication 24 August 2022, date of current version 14 September 2022.

Digital Object Identifier 10.1109/ACCESS.2022.3201343

RESEARCH ARTICLE

Design and Analysis of Ultra-Precise Large Range Linear Motion Platforms Using Compliant Mechanism

TANKSALE ABHIJIT AND GANDHI PRASANNA, (Member, IEEE)
Department of Mechanical Engineering, Indian Institute of Technology Bombay, Mumbai 400076, India

Corresponding author: Gandhi Prasanna (gandhi@iitb.ac.in)

This work was supported in part by the Science and Engineering Research Board of India under Grant CRG/2019/005615.

ABSTRACT Double parallelogram compliant mechanism (DPCM) is extensively used to obtain precise straight-line motion. Symmetric DPCMs, used previously, traverse a straight-line path without parasitic error when gravity vector is perpendicular to the plane of bending of beams. However, when gravity vector is either in line with beams (orientation B) or in the plane of bending of beams (orientation C), asymmetry in the loading causes undesired deviation from a straight-line path. This undesired deviation called parasitic error increases, especially in beams with relatively low flexural rigidity required to obtain larger displacements with low power actuators. This paper first characterizes parasitic error, in such cases, using large deformation analysis and further proposes novel ways to minimize it. A recently developed, chained beam constraint method is used to model, characterize, and optimize DPCMs. Optimized parameters are further validated by FEA and experiments. In orientation B, after implementing the proposed method, numerical analysis and experimental results show that the undesired parasitic error of 123 µm is drastically reduced to 2 µm and 6 µm, respectively. Moreover, systematic design procedure with corresponding graphs is presented to avoid modeling and optimization steps for a user-specific case. The proposed methods pave pathways to reducing the parasitic error during large-range motion using multiple orientations of DPCMs and thus make DPCMs more employable in several precision motion applications such as 3D optical scanners, 3D micro-printers, CMM probes, and microscopy stages.

INDEX TERMS Compliant mechanism, optimization, parasitic error, precise straight-line motion.

I. INTRODUCTION

Compliant mechanisms induce entire motion through deformation of flexible members or flexible joints which eliminate wear, friction, lubrication, and backlash [1]. Thus, compliant mechanisms provide backlash-free and friction-free smooth motion with precision, accuracy, repeatability, and reliability for many nano and microscale applications [2], [3], [4], [5], [6], [7], [8]. These mechanisms are used in applications such as microstereolithography [9], spontaneous fabrication of the 3D multiscale fractal structures [10], and semiconductor wafer inspection/production instrumentation [11], Micro-Electro-Mechanical Systems (MEMS) [12], Scanning Probe Microscopy (SPM) [13].

DPCM is one of the most widely used mechanisms in precision motion applications [14], [15], [16]. Traditionally DPCMs in a symmetric configuration are operated in orientation A (see Fig. 1(a)) with gravity vector perpendicular to the axis of the beams [17], [18], [19]. It is easier to accomplish ultra-precise straight-line motion using DPCMs operating in orientation A; the effect of gravity is ignorable on the motion of the mechanism. However, there could be a requirement either from loading capacity perspective or from a space availability perspective in applications where DPCM in other possible orientations B and C (shown in Fig.1(b) and (c)) would need to be used. In orientation B, the axial loading symmetry between outer and inner beams is broken since

The associate editor coordinating the review of this manuscript and approving it for publication was Jingang Jiang.

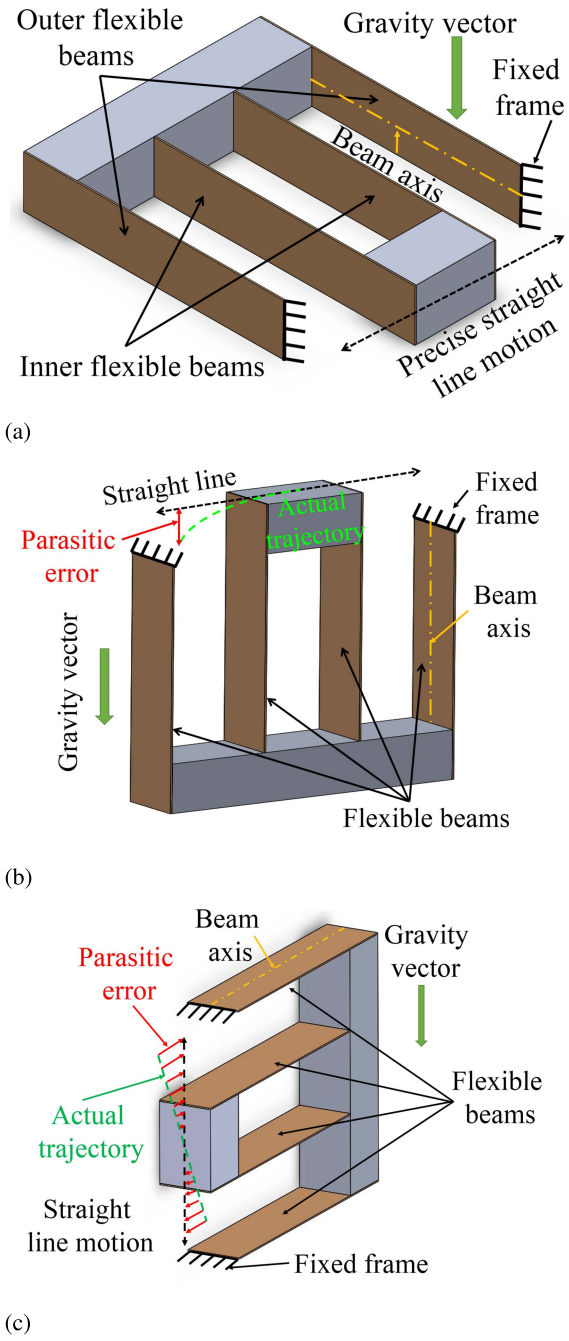

FIGURE 1. DPCM in (a) orientation A (b) orientation B (c) orientation C.

outer beams see tensile load while inner beams are loaded in compression. Axial loads (tensile in outer and compressive in inner) coupled with large bending deformations cause additional position dependent bending moments which induce significant nonlinear parasitic errors in the axial direction in this case. Orientation B eliminates the possibility of warping of flexible beams during deformation as the axial load due to gravity acts along the length of the beam. Unlike in orientation A, twisting loads are not induced in orientation B even after large deformation. In contrast, flexible beams in orientation A are more prone to warping during deformation due to parasitic twisting caused by the vertical load of stages and their reaction components. Orientation B has more load-carrying capacity than orientation A for the same stiffness in the direction of actuation. The orientation C is beneficial for obtaining motion in the vertical direction (along the gravity), which is impossible with other orientations B and C. In orientation C, the gravity vector is in-line with the bending direction of flexible beams; therefore, gravity load induces additional pure bending moments (deformation independent) in flexural beams without any axial load. Further, due to different static deflection of inner and outer beams, the parasitic error is always present in orientation C. The gravitational load significantly increases the parasitic error of DPCMs operating in orientation B and C. This study aims at eliminating or minimizing this parasitic error and obtaining highly precise straight-line motion over the large range of stroke with DPCM operating in orientations B and C. Few works of literature [20], [21], present ideas to to fix the motion ratio as 2:1 between primary and intermediate mass using slaving mechanism. The slaving uses an additional linkage to connect the primary and intermediate stage. Although this reduces undesired effects of axial forces to some extent, additional actuator forces are required in the direction of motion.

As the aim of this study is to achieve straight-line motion over the large range, consideration of the large deformation of flexible beams in the mathematical model is necessary. In literature, various models for the analysis of flexible beams with large deformations have been presented. Elastica theory is the method which delivers an exact solution to large deflections [22]. However, due to its non-closed-form nature (solution in terms of elliptic integrals), it is not suitable in the synthesis of mechanisms. Pseudo-rigid-body model (PRBM) initiated by Midha and Howell [1] is another technique utilized to evaluate the large deflection of flexible beams. PRBM is sensitive to loading condition, change in load due to extra force or moment demands for generating a new pseudo-rigid-body model via the optimization process. In the cases under consideration here (orientations B and C has shown in Fig. 1(b) and (c)), the loading conditions change continuously as a function of deformation. The other disadvantage of PRBM which arises due to lumped parameter approximation is an inaccurate slope at the end of the beam and inability to capture the elastic and elasto-kinematic effects along the axial direction. The recent advancement in modeling large deformation of the compliant mechanism includes energy minimization based solutions. Su and Turkkan [23] presented a method based on the minimum potential energy principle and optimization. This method uses any beam model with a closed-form energy equation in the minimization framework. The accuracy of this method depends on the accuracy of the beam model used in the framework. Chen and Ma [23] also presented an energy-based modeling framework for compliant mechanisms. Their future aim is to include the principle of minimum potential energy. Few recent works [24], [25] have presented models for planar compliant mechanisms applicable for small deformations only. Chained beam

constraint model (CBCM) is a new technique proposed recently by Ma and Chen [26], for analyzing large deflections of planar flexible beams. In CBCM, a flexible beam is discretized into a few elements, and then beam constraint model (BCM) is applied to each of these elements. BCM is based on a polynomial approximation to elastica theory. The advantages of BCM are that it provides compact, closed-form relations between end loads and end displacements. BCM captures the geometric linearities associated with planar beam flexure, load stiffening effect and elasto-kinematic effects [27]; consequently, CBCM takes these significant effects into account. However, BCM does not predict accurate results when deformation is more than 10% of the length of the beam. Therefore, CBCM plays a vital role in capturing large flexure deformations (more than 10%). In contrast to most other techniques, CBCM considers axial strain resulting from the axial load, capable of predicting deflection with the high compressive load. In comparison to FEM, CBCM requires very few elements to model the large deflection of flexible beams because of the capability of each element to capture intermediate deflection accurately and thus reduces time to reach accurate solution. Hence, CBCM is suitable for analysis and proposed optimization of parasitic error in the DPCMs operating in orientation B and C.

This article first analyzes DPCM operating in orientation B (to predict parasitic error), considering the combined effect of bending and axial gravitational load, along with experimental and FEA validation. Subsequently, it investigates DPCM operating in orientation C using CBCM and FEA, where the effect of additional bending moments due to gravitational load on the motion of mechanism is significant. Based on the analysis, we further propose a novel approach to achieve ultra-precise straight-line motion over a large range for DPCMs operating in both the orientations (B and C) by minimizing parasitic error with respect to different flexible beam parameters like width, thickness, and length. The optimization problem considers the stress constraint during deformation of flexible beams to avoid beams' failure due to fatigue. Finally, this paper proposes design steps to obtain optimized beam dimensions directly using a few equations and nondimensional graphs for DPCMs operating in orientation B. The results presented in this article can be extended to other configurations or orientations, where the effect of loads acting on mechanisms is similar to gravity. The proposed design procedure reduces the effort of the designer to get the optimized dimensions. The proposed linear motion platforms are useful as precision motion stages in applications like micro 3D printing [28], non-contact micro-machining equipments [29], [30], and non-contact metrology, to name a few. The other applications are precise guidance or measurement in optical systems [30], non-contact scanning, CMM probes, and microscopy stages.

II. MODELING OF DPCM

A nonlinear mathematical model for DPCM operating in orientations B and C is presented in this section. Primarily detailed modeling for orientation B has been explained. Modeling for orientation C remains the same; except a change in load equilibrium equations. The load equilibrium equations for orientation C are presented in Appendix C. DPCM under consideration here, operating in orientation B, consists of 8 flexible beams and two rigid masses. The intermediate mass (ms_1) is connected to ground through four flexible outer beams forming an outer parallelogram. Similarly, four inner beams connected to intermediate mass (ms_1) and primary mass (ms_2) forms an inner parallelogram. The DPCM is symmetric about mid-plane (see Fig. 25 in Appendix A). Theoretically, DPCM has geometrical symmetry, material symmetry, and symmetric boundary conditions about the mid-plane. Therefore, only half-portion of the mechanism is considered for modeling purposes, as shown in Fig. 2. This assumption simplifies the mathematical model and reduces the computational cost. It also makes the mathematical model easier to understand.

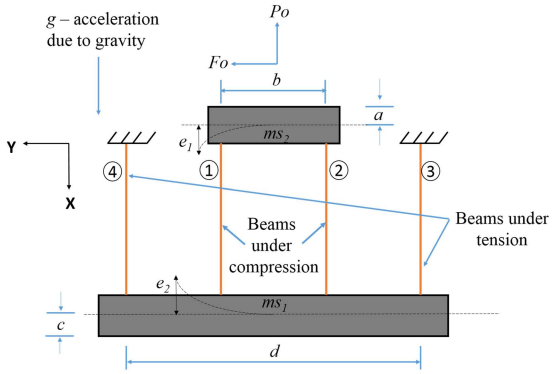

FIGURE 2. Double parallelogram compliant mechanism [31].

A. CHAINED BEAM CONSTRAINT MODEL

A chained BCM method [26], recently developed for modeling compliant mechanisms, is adopted here for modeling DPCM. A brief outline of modeling procedure is given in this section for the sake of completeness. CBCM discretizes flexible beams in compliant mechanisms into a few numbers of elements (see Fig. 26 in Appendix A) and each of these elements is modelled using BCM. BCM developed by Awtar *et al.* [32] accurately predicts intermediate deflection (within 10% of the length of the beam) of a flexible beam. BCM is capable of capturing geometric nonlinearities associated with an intermediate transverse deflection. Equation (1) and (2) represent the relations between end load and end displacement specified by BCM in the non-dimensional form [32]:

$$\begin{bmatrix} f \\ m \end{bmatrix} = \begin{bmatrix} g_{11} & g_{12} \\ g_{21} & g_{22} \end{bmatrix} \begin{bmatrix} \delta_y \\ \alpha \end{bmatrix} + p \begin{bmatrix} k_{11} & k_{12} \\ k_{21} & k_{22} \end{bmatrix} \begin{bmatrix} \delta_y \\ \alpha \end{bmatrix} + p^2 \begin{bmatrix} q_{11} & q_{12} \\ q_{21} & q_{22} \end{bmatrix} \begin{bmatrix} \delta_y \\ \alpha \end{bmatrix}, \quad (1)$$

$$\delta_x = \frac{t^2 p}{12L^2} - \frac{1}{2}\begin{bmatrix}\delta_y & \alpha\end{bmatrix}\begin{bmatrix}k_{11} & k_{12}\\ k_{21} & k_{22}\end{bmatrix}\begin{bmatrix}\delta_y\\ \alpha\end{bmatrix} - p\begin{bmatrix}\delta_y & \alpha\end{bmatrix}\begin{bmatrix}q_{11} & q_{12}\\ q_{21} & q_{22}\end{bmatrix}\begin{bmatrix}\delta_y\\ \alpha\end{bmatrix}, \quad (2)$$

where,

$$f = \frac{FL^2}{EI}, \quad p = \frac{PL^2}{EI}, \quad m = \frac{ML}{EI},$$
$$\delta_y = \frac{\Delta_y(L)}{L}, \quad \delta_x = \frac{\Delta_x(L)}{L}, \quad x = \frac{X}{L},$$

are the normalized load and deflection parameters of the beam. The non-dimensional beam characteristic coefficients *g's, k's* and *q's* are given in Table 3 in Appendix A. BCM considers the effect of geometric nonlinearity due to arc length conservation and the effect of nonlinearity due to curvature on the deflection of planar beam flexure undergoing intermediate deflection. It also takes into account the effect of axial force on the deflection of a flexible beam.

In CBCM [26] transfer of loads from one element to the next is carried out using the following equations of load equilibrium for the j^{th} element

$$\begin{bmatrix}\cos\theta_j & \sin\theta_j & 0\\ -\sin\theta_j & \cos\theta_j & 0\\ 1+\delta_{xj} & -\delta_{yj} & 1\end{bmatrix}\begin{bmatrix}f_j\\ p_j\\ m_j\end{bmatrix} = \begin{bmatrix}f_{j-1}\\ p_{j-1}\\ m_{j-1}\end{bmatrix}. \quad (3)$$

The geometric constraints stated by CBCM [26] for the whole beam are

$$\sum_{j=1}^{N}\left[\begin{bmatrix}\cos\theta_j & -\sin\theta_j\\ \sin\theta_j & \cos\theta_j\end{bmatrix}\begin{bmatrix}L_j(1+\delta_{xj})\\ L_j\delta_{yj}\end{bmatrix}\right] = \begin{bmatrix}X_0\\ Y_0\end{bmatrix},$$
$$\theta_N + \alpha_N = \theta_0, \quad (4)$$

where, L_j is the length of the j^{th} element and $L_j = L/N$ for equal discretization. Equation (1) and (2) obtained from BCM for all elements, along with load equilibrium and the geometric constraint presented in (3) and (4) respectively, constitutes the CBCM model for a beam undergoing large deformation. If three load parameters (P_o, F_o, M_o) are known, then the remaining three deflection parameters (X_o, Y_o, θ_o) are found out by numerically solving the CBCM equations or vice versa.

B. STATIC ANALYSIS OF DPCM

DPCM under consideration consists of four flexible beams, as shown in Fig. 2. Each flexible beam is further divided into six equal elements using CBCM to make sure that deflection of every element is within 10% of the length of the element. Further, 3 equations presented in (1) and (2) of BCM are applied to each of the six elements would give 18 equations pertaining to the load displacement relationships. The load equilibrium equations presented in (3) are applied to these elements would give additional 15 equations. In addition, 3 geometric constraint equations are given by (4). Besides, three extra equations are formed, to transform the known load in the global coordinate frame (F_o, P_o and $M_o = 0$) to last elements local coordinate frame. Thus, a flexible beam with

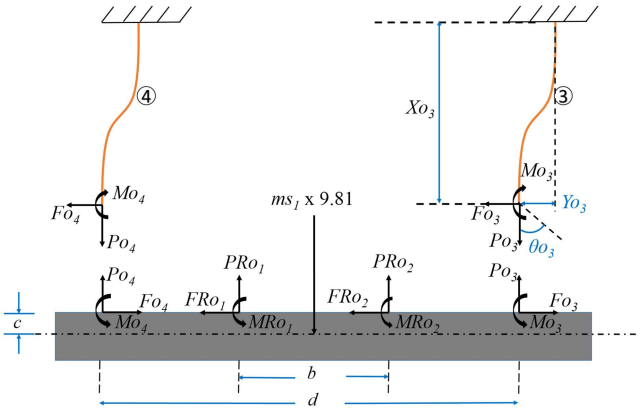

FIGURE 3. Free body diagram of Intermediate mass [31].

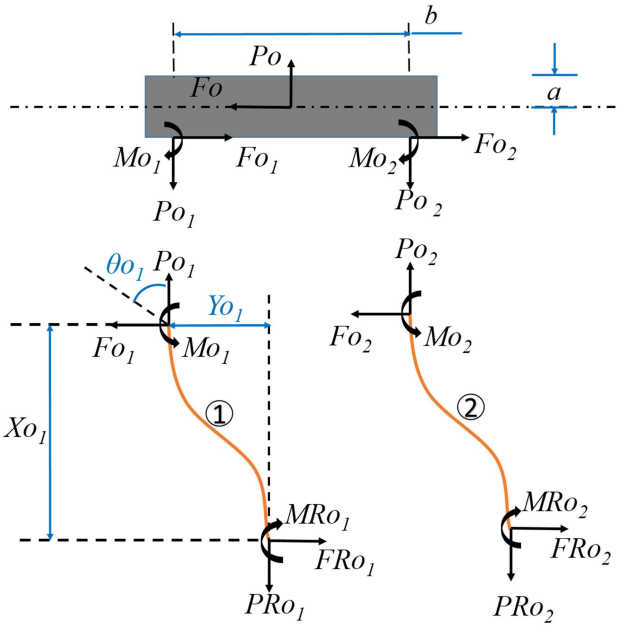

FIGURE 4. Free body diagram of primary mass [31].

six elements require 39 nonlinear equations to model large deformation with CBCM. Total, 156 (39 × 4) equations are formulated for DPCM with four beams by applying CBCM. Two rigid-body masses attached to flexible beams are also constituent elements of DPCM. This attachment of masses to flexible beams impose certain geometric constraints on the beams and also transfers the load to the beams. Free body diagrams of intermediate mass and primary mass for orientation B are shown in Fig. 3 and 4, respectively.

Equation (5) is obtained by applying load equilibrium to primary mass ms_2.

$$Fo - Fo_1 - Fo_2 = 0,$$
$$Po - Po_1 - Po_2 = 0,$$
$$(Fo_1 + Fo_2)a + Po_1\left(\frac{b}{2}\right) = Po_2\left(\frac{b}{2}\right) + Mo_1 + Mo_2. \quad (5)$$

The geometric constraints for primary mass ms_2 are given by

$$\begin{aligned} \theta o_1 &= \theta o_2, \\ Xo_1 &= Xo_2 - b\sin(\theta o_1), \\ Yo_2 &= Yo_1 + b - b\cos(\theta o_1). \end{aligned} \tag{6}$$

Similarly, (7) is obtained by applying load equilibrium to intermediate mass ms_1.

$$\begin{aligned} Fo_3 + Fo_4 &= FRo_1 + FRo_2, \\ PRo_1 + PRo_2 &= ms_1(9.81) - Po_3 - Po_4, \\ PRo_1\left(\frac{b}{2}\right) + Po_4\left(\frac{d}{2}\right) &= PRo_2\left(\frac{b}{2}\right) + Po_3\left(\frac{d}{2}\right) \\ &\quad -(Fo_3 + Fo_4)c \\ &\quad +(FRo_1 + FRo_2)c \\ &\quad +MRo_1 + MRo_2 \\ &\quad +Mo_3 + Mo_4. \end{aligned} \tag{7}$$

The geometric constraints on intermediate mass ms_1 are

$$\begin{aligned} \theta o_3 &= \theta o_4, \\ Xo_4 &= Xo_3 - d\sin(\theta o_3), \\ Yo_3 &= Yo_4 + d - d\cos(\theta o_3). \end{aligned} \tag{8}$$

Finally, 168 nonlinear equations consisting of load equilibrium conditions (5) and (7), CBCM equations, and geometric constraints (6) and (8) are numerically solved using "fsolve" (nonlinear system solver) in *MATLAB* to find 168 unknowns. These unknowns consists of nondimensional parameters $f, p, m, \delta_y, \delta_x, \alpha$ of each element (thus a flexible beam with six elements contain 36 local unknowns), along with Fo_x, Po_x, Mo_x, Xo_x, Yo_x and θo_x as a global unknowns (x indicates beam number). Therefore, the total number of unknowns per beam become 42, which leads to 168 unknowns for a DPCM consisting of 4 such beams. A different set of load equilibrium conditions as in (5) and (7) would be obtained for DPCM in orientation C. All other equations would remain the same. The load equilibrium equations for primary mass and secondary mass of DPCM operating in orientation C are presented in Appendix C.

After solving the above simultaneous equations for given loads (F_o, P_o, M_o) and initial dimensions of the inner and outer beam, we obtain the solution in terms of elemental level deformations. From these elemental solutions, global solution for complete deformation profile for each of the beams is computed. Particularly the tip deformation in the axial direction for each beam gives its own parasitic error. The total parasitic error (e) is further obtained by subtracting individual parasitic errors of inner and outer beams as follows:

$$\begin{aligned} e &= e_1 - e_2, \\ &= (L_i - Xo_1) - (L_o - Xo_3). \end{aligned} \tag{9}$$

This error will be used for further analysis and proposed optimization in subsequent sections.

C. MINIMIZATION OF PARASITIC ERROR

This section presents novel ideas for minimization of parasitic error in the proposed orientations B and C, respectively. Furthermore, it develops physical insights into how the concepts presented lead to the minimization of the error. Interestingly, it is found that orientations B and C require a completely different set of ideas that would work for minimization of parasitic error.

1) DPCM OPERATING IN ORIENTATION B

For DPCM operating in orientation B, gravity effects play a dominating role in creating asymmetry in the loading. Therefore, the motion of the stage will not be in a straight line as intended because of parasitic error in X-direction. The specific results of DPCM operating in orientation B are presented in Fig. 8 in Section IV-A later. We formulate optimization problem here to address the following question: Are there set of beam parameters which will induce some asymmetry in the structure in such a way that the motion of the platform is still in a straight line eliminating parasitic error? In particular, for a set of inner beam parameters, we look at the change in width, thickness or the length of outer beams, one at a time, keeping other values the same, for minimization of parasitic error over entire desired stroke.

Hence, we define the optimization objective function f as

$$f(x) = \sum_{i=1}^{N} [e_i - e_0]^2, \tag{10}$$

where, $i = 1, 2, \ldots, N$ are the applied load steps and e_0 is parasitic error at zero transverse force.

The e_0 indicates the component of parasitic error because of axial deformation of beams due to gravity even without applying any transverse force. This component e_0 can be considered as a new reference point to achieve straight-line motion in the xy plane, passing through the point(0, e_0) and having equation as $y = e_0$ (y direction is along the direction of gravity). With this understanding, we formulate objective function f by subtracting e_0 in order to minimize further variations of parasitic error. The optimized trajectory traced by motion stage, with and without consideration of e_0 in the objective function is shown in Fig. 27 in the Appendix A.

Considering various parameters to be optimized and constraints thereof, we propose the following mathematical formulation of the optimization problem:

$$\begin{aligned} &\underset{x}{Minimize}\, f(x), \\ &Subjected\ to\ x_{min} \le x \le x_{max}; \\ &\qquad \sigma_{max} \le S_e. \end{aligned} \tag{11}$$

Design variable (x) is one of the outer beam parameters like L_o, t_o or W_o, and it should be positive and within some bounds x_{min} and x_{max}. For the optimization problem under consideration, the minimization of objective function f can only be obtained by reducing the transverse stiffness of outer beams and making it equal to or close to the transverse stiffness

of inner beams. Suppose thickness (t_o) or width (W_o) is the design variable (x). The stiffness of outer beams can only be reduced by reducing the thickness or width value compared to inner beams. Therefore, the upper bound limit for x is the corresponding thickness (t_i) or width (W_i) of the inner beam, and the lower bound can be any positive value close to zero. When the length (L_o) is the design variable, the stiffness of outer beams can only be reduced by increasing the length of outer beams. Therefore, the lower bound for x is the length (L_i) of the inner beam and the upper bound is obtained by trial and error such that the minimum value of the objective function falls within two bounds. The constrained optimization problem presented in (11) is solved using *MATLAB*. The results of DPCM after optimization of parasitic error are discussed in Section IV-A3 later.

2) DPCM OPERATING IN ORIENTATION C

In the case of DPCMs operating in orientation C, gravity loads due to stage masses are in the direction of bending of beams rather than in axial direction as in orientation B. Furthermore bending of inner beams (in addition to that caused by applied force) is caused by gravity load of only the primary stage however in bending of outer beams, both primary and intermediate stage masses participate. Thus initial equilibrium position has some parasitic error contributed by asymmetric bending of inner and outer beams. Asymmetry continues further as we apply external force F_o leading to large parasitic errors in following straight line. Changing beam parameters alone will not change this variation significantly to reduce parasitic error. Hence a novel approach is proposed here to resolve this issue. In this approach, we proposed to attach two separate tension springs (always in tension throughout the desired stroke) at primary and secondary mass such that these springs will nullify the static deflection of inner and outer beams (see Fig. 5). This will make sure that the DPCM will not have any static deflection when the external force applied is zero. After attaching the external springs such that $k_1x_1 = ms_1g$ and $k_2x_2 = ms_2g$ and then optimizing the beams for a new situation gives the desired precision in traversing straight line. The mathematical formulation of the optimization problem in this orientation is the same as orientation B (presented in (11)), except for a small change in the objective function. The objective function f for orientation C is

$$f(x) = \sum_{i=1}^{N} [e_i]^2. \tag{12}$$

The component e_0 of parasitic error is not present in (12) because there is no axial load on the flexible beams in this orientation. As well as the parasitic error due to static deflection has been nullified by attaching the external springs. The results of DPCM after applying the proposed strategy are discussed in Section IV-B2. The initial stretch x_1 and x_2 from their respective free lengths (x_0) decide the spring stiffness k_1 and k_2, respectively. The smaller the initial stretch of the spring, the required stiffness of the spring is large and vice versa. Suppose the stiffness of the springs is more, the overall motion stiffness increases, leading to more actuator power for a particular range of motion. Therefore, it is advisable to use springs with lower stiffness values by keeping the initial stretch as maximum as possible. The initial stretches have to be $x_1 > stroke$ and $x_2 > \frac{stroke}{2}$ to satisfy the necessary condition that both the springs must always be in tension.

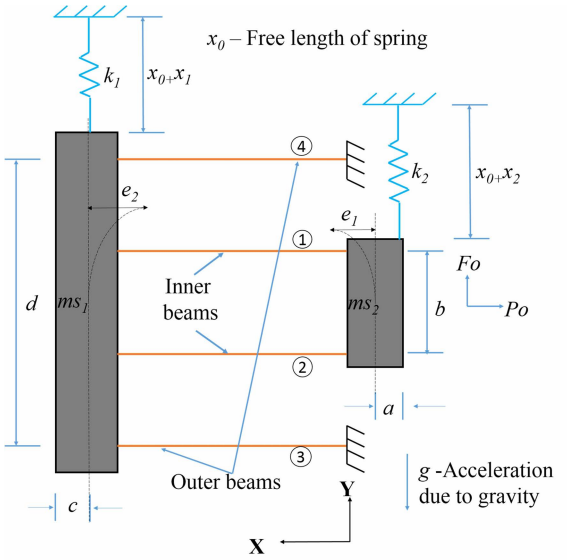

FIGURE 5. DPCM operating in orientation C.

III. FEA AND EXPERIMENTAL DETAILS

The CBCM based simulations predicted that the proposed strategies substantially reduced the parasitic error over the entire stroke for both the orientation B and C (Results are discussed in Section IV later). To cross-verify the CBCM results, Finite element analysis (FEA) has been carried out using ANSYS 16.2 workbench. The hexahedron elements are used along with 1% convergence on the displacement in the transverse direction. The convergence criteria have been applied to displacement because deformation of beams is more significant in this study.

Further, experimental work is carried out on a fabricated prototype of DPCM operating in orientation B to validate the effectiveness of the proposed method and optimization. Schematic, along with actual experimental setup, is shown in Fig. 6 and 7, respectively. For orientation B, experimental results are in good agreement with CBCM and FEA results. Orientations B and C are structurally alike and have similar loading conditions (transverse load and no twisting load induced during deformation due to stage masses). Hence, the proposed methodology for orientation C is validated using FEA and CBCM results.

Table 1 shows the various parameters of the fabricated double parallelogram compliant mechanism before and after optimization. The guidelines provided by Gandhi *et al.* [33]

TABLE 1. Parameters of DPCM.

	Length (mm)	Width (mm)		Thickness (mm)	Material (Beryllium Copper)
		unoptimized	optimized		
Outer beams	109	28	15.26	0.5	E=130 Gpa
Inner beams	109	28	28	0.5	E=130 Gpa
Mass properties					
$ms_1 = 1.325$ (kg)					
$ms_2 = 2.267$ (kg)					

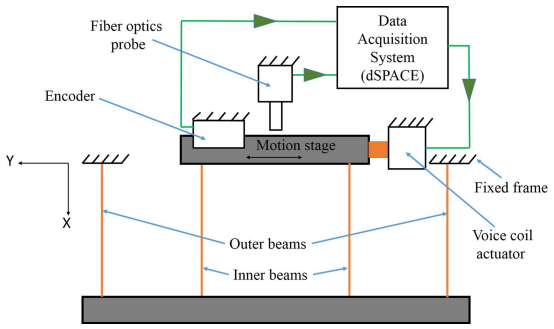

FIGURE 6. Schematic diagram of experimental setup [31].

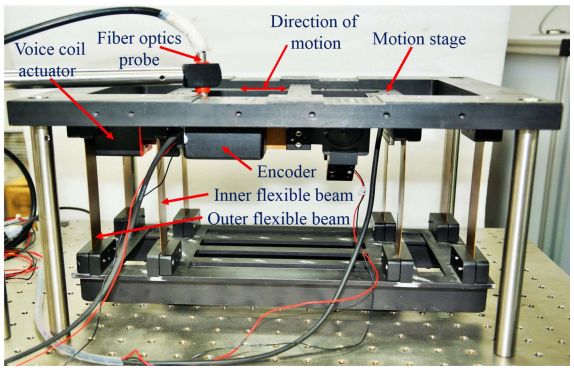

(a) Front view

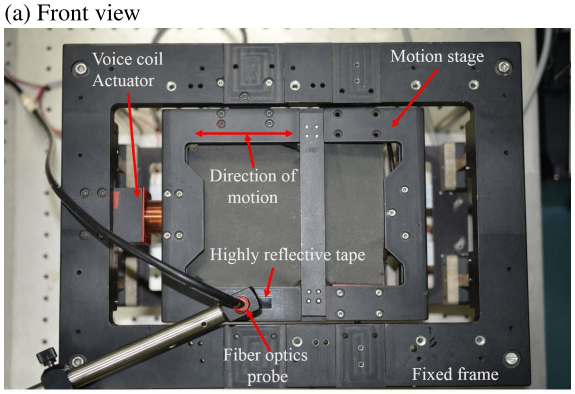

(b) Top view

FIGURE 7. Experimental setup of double parallelogram compliant mechanism.

are followed to build a warp-free assembly of spatial double parallelogram compliant mechanism using the flexible members and rigid masses. The experimental parasitic error along X-axis and transverse displacement of motion stage along Y-axis is measured through fiber optics probe (Philtek RC 140) and optical encoder (Renishaw V2BBI30D50B), respectively. Reading of encoder and fiber optics probe, along with actuation of the voice coil actuator (BEI Kimco LA15-26-000A) to move the motion platform is performed through the dSPACE 1103 DAQ system.

IV. RESULTS

Results obtained before and after applying the proposed novel ideas are presented in this section for both the orientations B and C. The results are discussed separately for DPCMs operating in orientation B and C under the Section CASE I and CASE II, respectively. The experimental results presented in this study are an average of 3 groups of sample data.

A. CASE I: DPCM OPERATING IN ORIENTATION B

1) CHARACTERIZATION OF UNOPTIMIZED DPCM

The trajectory of the motion stage of DPCM, before optimization, predicted by model along with experimental and FEA results, is shown in Fig. 8. As expected, we observe the gradual nonlinear increase in parasitic error in the axial X direction as a function of transverse deformation in Y direction, maximum being 123 µm over a range of +/− 10 mm. Further, we observe that parasitic error is a result of uncompensated axial deformations of inner and outer beams. Fig. 8 shows that the path of the motion stage predicted by the mathematical model under the given loading condition is very close to FEA and experimental results.

Owing to different axial forces in outer (tension) and inner (compression) beams, the axial deformations in these beams at any given transverse force F_o are going to be different. This difference in axial deformations at an applied force is observed in Fig. 9, which presents individual parasitic errors of inner and outer beams.

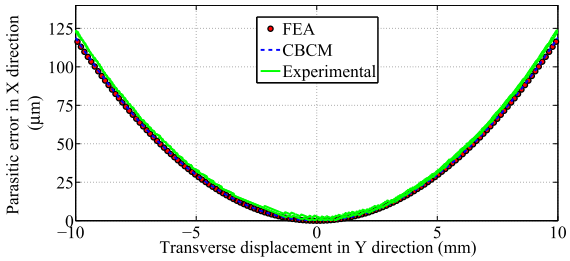

FIGURE 8. Trajectory of motion stage before optimization.

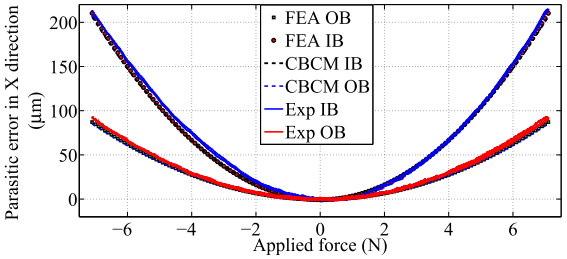

FIGURE 9. Force against parasitic error.

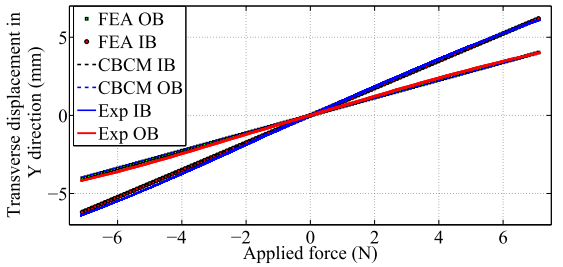

FIGURE 10. Force against transverse displacement.

Thus, these axial deformations would not compensate for each other (although in the opposite direction) as in the case of DPCM in orientation A and would result in the parasitic error we observe in Fig. 8.

Another way to look at these results is from transverse deformation perspective. Fig. 10 shows transverse deformations of inner and outer beams, all having identical parameters, as the applied force F_o is increased. The difference in transverse deformation we observe is due to the differential effect of axial forces in these beams. We can see from BCM equations that for a constant axial force in this case, axial static deformations 'δ_x' of both inner and outer beams is identically, nonlinearly related to transverse deformations 'δ_y'. Thus the parasitic error is a natural result of different transverse deformations of these beams as observed in Fig. 10. The error between experimental and simulation results are shown in Fig. 28 and 29 in Appendix A for parasitic error and transverse displacement, respectively.

2) SELECTION OF BEAM PARAMETER FOR OPTIMIZATION

It is clear that when all the beam parameters are identical for inner and outer beams, motion stage has an undesired parasitic error due to axial (gravitational) load experienced by inner and outer beams. This parasitic error can be minimized by varying at least one of the flexible beam parameters width, thickness, or length. The effect of each beam parameter on the parasitic error of motion stage is different. Fig. 11 shows the value of objective function given by (10) against variation of the outer beam parameters while other parameters are kept constant and equal to inner beam parameters. It is clear from Fig. 11 that the objective function has a minimum value in case of width as compared to other beam parameters which are thickness and length. Therefore, optimization of width is preferred as compared to optimization of other beam parameters. Moreover, experimentally it is also easier to reduce the width of the flexible beam and practically implement it into the experimental setup of DPCM. Hence, the width of the flexible beam selected as a design variable for optimization.

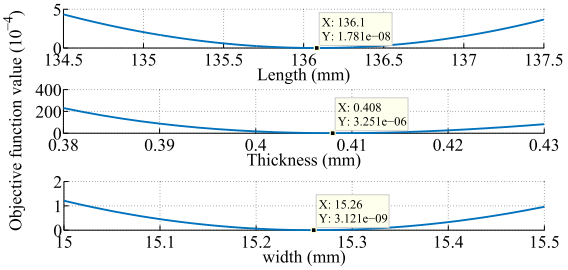

FIGURE 11. Objective function value against beam parameters.

3) CHARACTERIZATION OF OPTIMIZED DPCM

The trajectory traced by motion stage, after optimization of the width of the outer beams is shown in Fig. 12. CBCM and FEA results show that the parasitic error in X direction has drastically reduced from 123 µm to less than 1 µm and 2 µm, respectively after optimization. However, the experimental parasitic error is around 6 µm. This deviation between experimental and model predicted parasitic error is due to manufacturing and assembly errors associated with the experimental setup.

After optimizing width of the outer beams, transverse deformation of inner and outer beams, along Y direction is almost identical for each and every load step applied as shown in Fig. 13. The axial load on beams, when tensile, increases transverse stiffness and when compressive, decreases it because of change in direction of additional bending moment it contributes during deformation. Optimization process adjusts the beam stiffnesses for this change. Particularly width of outer beams, which are in tension, is decreased as compared to inner ones to compensate for the effect so that the effective stiffness (considering axial force) of both beams is almost identical. Thus their deformations are identical at any point during motion. In addition, because of identical lengths of beams, the axial deformations of inner and outer beams also become identical (See Fig.14). Hence the total parasitic error is very close to zero. However, in the case of unoptimized DPCM the effective transverse stiffnesses

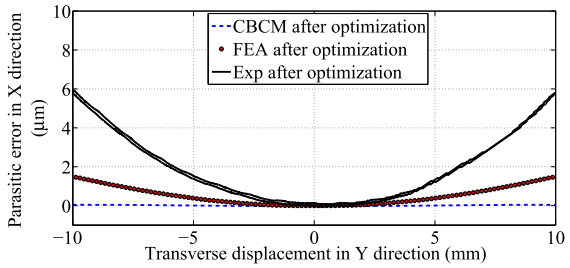

FIGURE 12. Trajectory of motion stage after optimization.

of inner and outer beams are different (even though beams are identical). The optimized width of the outer beam has a lower value than the unoptimized width (see Table 1) which means the transverse stiffness of outer beams has reduced compared to unoptimized DPCM. The reduction in the transverse stiffness of outer beams reduces the overall stiffness of DPCM after optimization, which results in less force/power requirement for a particular range of motion than unoptimized DPCM. Fig. 13 also shows that the maximum applied transverse force is 5.8 N, which is less compared to 7.1 N force required in case of unoptimized DPCM, for the same stroke of $+/-10$ mm as shown in Fig. 10. The error between experimental and simulation transverse displacement, as well as parasitic error, is shown in Fig. 30 and 31 in Appendix A, respectively.

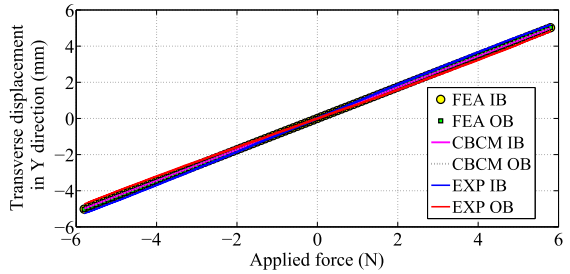

FIGURE 13. Force against transverse displacement.

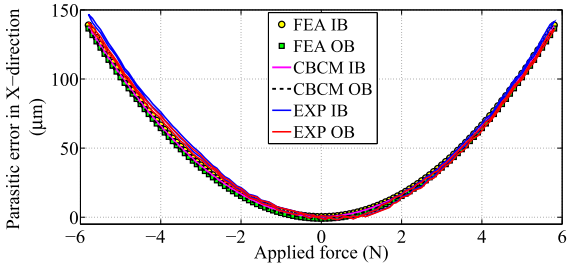

FIGURE 14. Force against parasitic error.

a: DESIGN STRESS

The CBCM based model of DPCM also predicts the maximum normal stress produced in the flexible beam under the applied loading condition. Note that shear stress is negligible as compared to normal stress. The prediction of maximum normal stress helps to design the flexible beams. Maximum stress generated in the beams should be less than the fatigue strength of the flexible beam material. The maximum normal stresses produced in the inner and outer beams of the optimized DPCM under the applied load are shown in Fig.15.

The maximum stress produced in the inner and outer beam is 79.49 MPa and 89.58 MPa, respectively. In both the beams, stress is less than the fatigue strength (275 Mpa) of the beam material. The maximum stresses in inner and outer beams predicted by CBCM are in good agreement with FEA results.

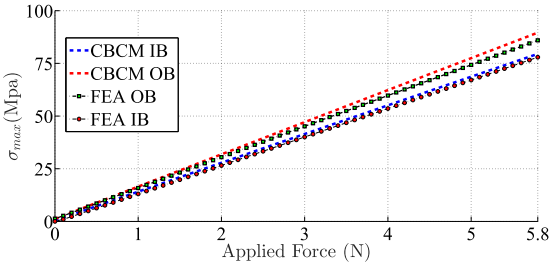

FIGURE 15. Maximum normal stress produced in inner and outer beam.

4) PROPOSED DESIGN STEPS FOR OPTIMIZED DPCM

For DPCMs operating in orientation B, a general design procedure has been formulated, in this section, to get optimized beam dimensions directly from few non-dimensional graphs and equations obtained from them. This procedure will be helpful in obtaining the optimized beam parameters without the need for writing or rerunning the code again for given specific case. The procedure to obtain optimized beam dimensions for few cases of thickness to length ratio $\left(\frac{t}{L}\right)$ and mass ratio $\left(\frac{ms_1}{ms_2}\right)$ is outlined below.

Step 1: Application requirements would define the following inputs required to design an optimized DPCM: the desired range of stroke (maximum motion on one side from mean position) and values of primary (ms_2) and secondary mass (ms_1). Once, these inputs are available; the designer can choose the length of the beams such that the stroke value is in between 1 to 40% of the length of the beam. Length of inner (L_i) and outer (L_o) beams are same and indicated as L.

Step 2: Find out the maximum allowable beam thickness value to avoid the fatigue failure of the beams for the selected length and desired stroke from (13). Equation (13) is derived from the graph shown in Fig. 16.

Select the appropriate value of thickness such that it is less than the t_{max} obtained from (13). Thickness is equal for both inner and outer beams and indicated as t.

$$\frac{S_e}{E} = 3\frac{stroke.t_{max}}{2L^2} \tag{13}$$

Step 3: Based on the thickness to length ratio $\left(\frac{t}{L}\right)$, stroke to length ratio $\left(\frac{stroke}{L}\right)$ and mass ratio $\left(\frac{ms_1}{ms_2}\right)$, get the value of non-dimensional stiffness difference (NSD) between inner

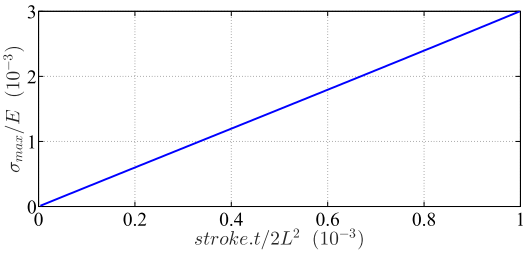

FIGURE 16. Strain against non-dimensional deformation.

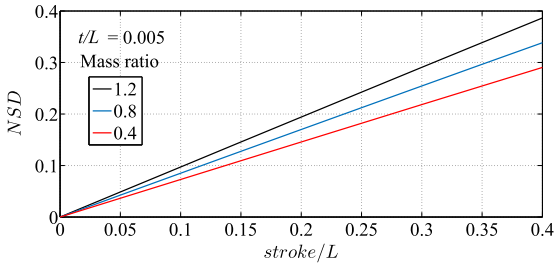

(a) Thickness to length ratio is 0.005

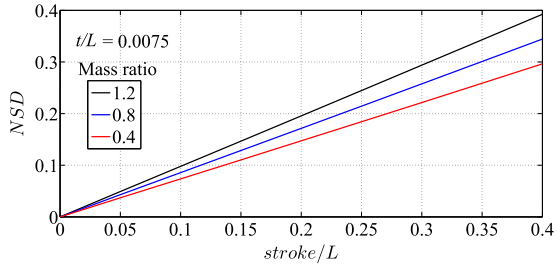

(b) Thickness to length ratio is 0.0075

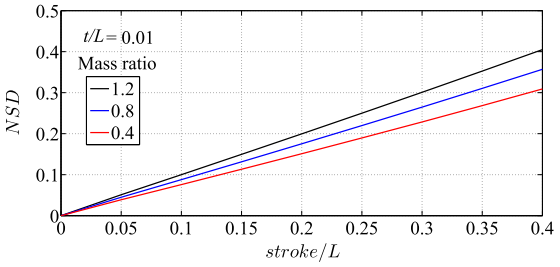

(c) Thickness to length ratio is 0.01

FIGURE 17. Non-dimensional stiffness difference against stroke to length ratio for different mass ratios.

and outer beams from the graph shown in Fig. 17. The more accurate value of *NSD* can be obtained using equations given in Table 4 in Appendix A. By substituting the values in (14), get the difference between the width of the inner and outer beams W_d^* where the value of primary mass (ms_2) is 1 kg.

$$NSD = \frac{E(W_d^*)t^3 \cdot stroke}{ms_2 gL^3} \tag{14}$$

Step 4: Calculate the actual width difference (W_d) for the desired mass using the graphs shown in Fig.18. The accurate value of W_d can be obtained using equations given in Table 5 in Appendix A, where $W_d = W_i - W_o$.

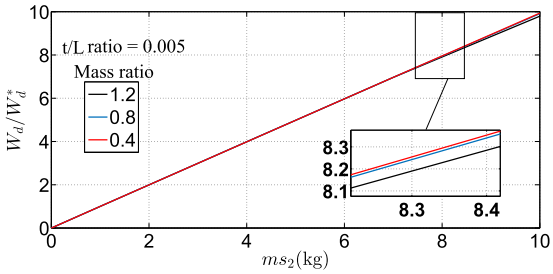

(a) Thickness to length ratio is 0.005

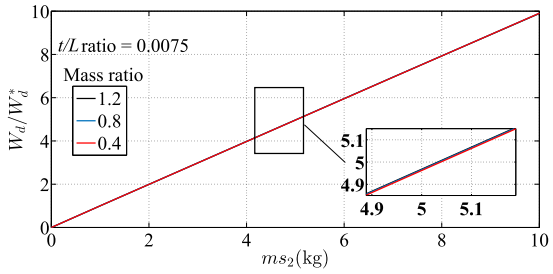

(b) Thickness to length ratio is 0.0075

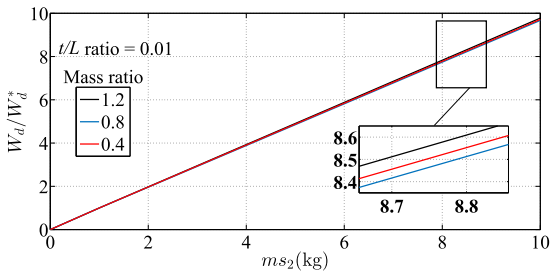

(c) Thickness to length ratio is 0.01

FIGURE 18. W_d/W_d^* against primary mass.

Step 5: The inner beams are under compression, which may lead to buckling failure of inner beams if not designed for buckling. After the selection of length and thickness, find out the minimum value for the width of inner beams to avoid buckling using (15):

$$(W_i)_{min} = \frac{3ms_2 gL^2}{\pi^2 Et^3}. \tag{15}$$

Select the value of the width of the inner beams such that it is higher than $(W_i)_{min}$ to avoid buckling of inner beams. Finally, we get the value of the width of the outer beams W_o by subtracting the difference between inner and outer beams (W_d), which we already got in previous Step 4.

This procedure is designed based on the fundamental understanding of variations and applicable to large range of beam dimensions for both small and large deformations. The illustrative example to carry out the proposed design procedure with sample case is explained in Appendix B.

B. CASE II: DPCM OPERATING IN ORIENTATION C

1) CHARACTERIZATION OF UNOPTIMIZED DPCM

Various parameters of DPCM operating in orientation C used for simulation are shown in Table 2. The trajectory of the

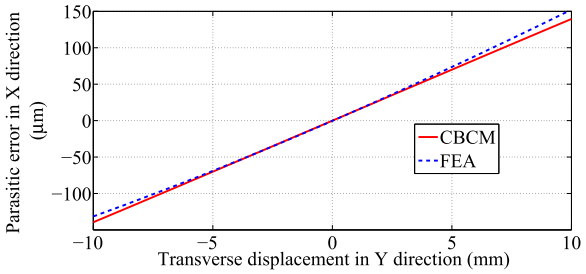

FIGURE 19. Path followed by motion stage before optimization.

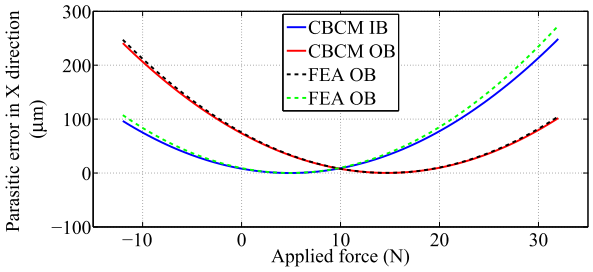

FIGURE 20. Force against parasitic error.

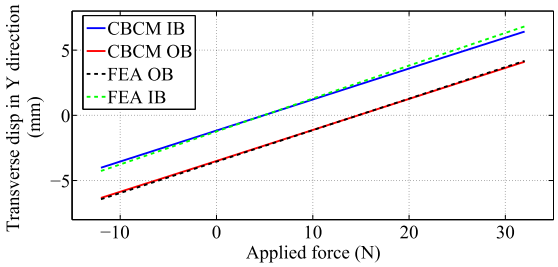

FIGURE 21. Force against transverse displacement.

motion stage of DPCM operating in orientation C, before optimization, predicted by the model and FEA, is shown in Fig. 19. The trajectory of the motion stage predicted by FEA and CBCM is nearly same up to the transverse displacement of $+/-$ 4 mm, as the displacement increases further, the error between trajectory predicted by FEA and CBCM increases. The maximum difference between FEA and CBCM predicted parasitic error is around 10 µm at 10 mm transverse displacement. We observe that the trajectory traced by the motion stage is inclined and has a gradual increase in parasitic error on both sides of mean position (zero transverse displacement). The parasitic error is positive on one side of the mean position and negative on another side of mean position (see Fig. 19). This means the motion stage (primary mass) moves in outward direction while traversing in the direction of gravity and vice versa. Parasitic error in axial X direction increases as a function of transverse deformation in the Y direction, the error becomes 140 µm over a range of $+/-$ 10 mm. In this case, the parasitic error is a result of asymmetric bending of inner and outer beams.

This asymmetric bending is due to asymmetric gravity load acting on the inner and outer beams which cause different axial deformation in inner and outer beams at every instant of the load. This causes the parasitic error of both the beams to be different even though both the beams are of identical dimensions (see Fig. 20). Due to different bending moments in outer and inner beams, the axial deformations in these beams at any applied transverse force F_o are going to be different (except one point where error curves cross each other) which can be observed in Fig. 20. Thus, these uncompensated axial deformations would result in the parasitic error we observe in Fig. 19.

Another perspective to understand these results is from transverse deformation of inner and outer beams. Fig. 21 shows transverse deformations of inner and outer beams, all having identical parameters, against the applied transverse force F_o. The asymmetric transverse deformation is a consequence of asymmetric bending of inner and outer beams due to gravitational load at any particular applied transverse force. This asymmetric transverse deformation leads to different parasitic error in inner and outer beams. The gravitational load is always acting on both the inner and outer beams; this can be observed from asymmetric static deformation of inner and outer beams present at zero transverse force. This constant gravitational load acting in the direction of gravity leads to different force requirements on both sides of zero transverse position. Therefore, the force required to achieve -10 mm (towards gravity) and $+10$ mm (opposite to gravity) stroke from the mean position is 12 N and 32 N respectively.

2) CHARACTERIZATION OF OPTIMIZED DPCM

The trajectory traced by motion stage, after attaching two separate springs to intermediate and primary mass with required stiffness (k_1 and k_2) and initial stretch (x_1 and x_2), and then optimizing width of the outer beams is shown in Fig. 22. The attached springs nullifies the static deflection of both the beams due to stage masses and brings DPCM to mean position. CBCM and FEA results show that the parasitic error in X direction has drastically reduced from 140 µm to less than 1 µm and 6 µm, respectively after attaching springs of required stiffness and further optimizing the width of outer beams. Optimizing outer beams after attaching the springs is required because the addition of springs makes the system configuration such that the transverse force experienced by inner and outer beams is not equal. The external transverse force applied to the primary mass act on both inner beams and spring with stiffness k_2 attached to mass ms_2. As the inner beams and spring of stiffness k_2 are in parallel configuration, the applied force is shared between them in the ratio which is present between their stiffness. The force experienced by inner beams gets transferred to intermediate mass. However, again, it is divided into two parts because intermediate-mass ms_1 and spring of stiffness k_1 are in parallel configuration. This indicates that the force experienced by outer beams is always less than the force experienced by inner beams. Hence

TABLE 2. Parameters of DPCM operating in orientation C.

	Length (mm)	Width (mm)		Thickness (mm)	Elastic modulus (Gpa)
		Unoptimized	Optimized		
Outer beam	100	20	17.6595	1	E=105
Inner beam	100	20	20	1	E=105
Mass properties			Spring properties		
$ms_1 = 1$ (kg)			$k_1 = 490.5$ (N/m)	$x_1 = 0.02$ (m)	
$ms_2 = 0.5$ (kg)			$k_2 = 490.5$ (N/m)	$x_2 = 0.01$ (m)	

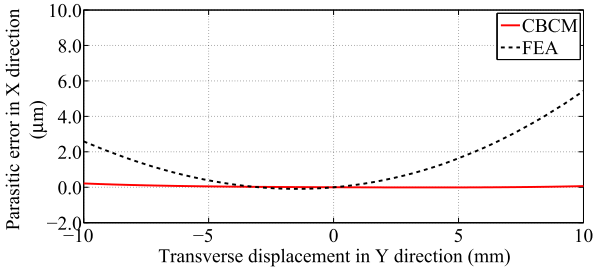

FIGURE 22. Path followed by motion stage after optimization.

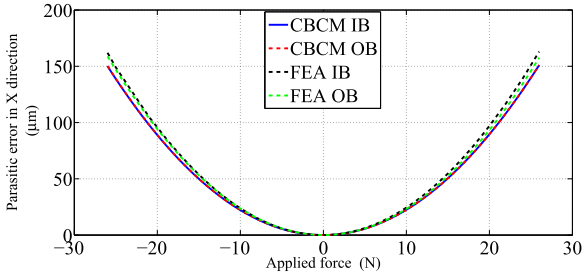

FIGURE 24. Force against parasitic error.

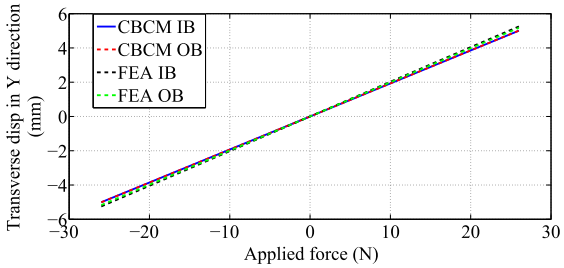

FIGURE 23. Force against transverse displacement.

stiffness of outer beams must be less than that of inner beams to obtain equal transverse deformation.

Fig. 21 clearly shows that for unoptimized DPCM, static deformation of inner and outer beam is 1.25 mm and 3.55 mm, respectively. A difference of 2.3 mm is observed between the initial static deformations of inner and outer beams. This difference between the transverse deformations remains nearly constant for the entire range of motion which leads to unequal axial deformations (parasitic errors) of inner and outer beams. However, there is zero static deformation in inner or outer beams after applying the proposed strategy. It is observed in Fig. 23 that the transverse deformations of inner and outer beams after optimization, along Y direction is almost identical for each and every load step. Therefore, the parasitic error experienced by the inner and outer beams gets indistinguishable for every load step (see Fig. 24). Hence, the total parasitic error reduces close to zero. The maximum force required on both sides of the mean position is 26 N for the stroke of $+/-$ 10 mm, which is slightly less than the 32 N force required for unoptimized DPCM for same stroke. This shows that with the proposed method, it is possible to obtain ultra-precise straight-line motion for DPCMs operating in orientation C.

V. CONCLUSION

This work proposed novel methods towards achieving a close to perfect straight-line motion using DPCM in configurations or orientations (B and C) amenable to several applications. The method minimizes parasitic error over the entire stroke with variation in beam parameters such as width, thickness, and length. Recently published CBCM was used to model the beam and optimize parameters on account of its computation effectiveness while capturing the large deformations. Results were further validated using an extensive set of experiments for orientation B. Moreover, optimization data is generalized in non-dimensional form, and a constructive procedure is outlined to design beams given the application requirements. The proposed design steps require neither modeling nor simulation and hence easily usable for quick design of optimized mechanisms. This work thus opens up possibilities in use of compliant motion platforms operating in different orientations for a much larger range of motion with an ultra-precise straight-line motion for corresponding applications. It is evident that by variation of parameters, it is possible to achieve nanoscale resolution in the straightness of motion.

TABLE 3. Beam characteristics coefficients of BCM matrices [32].

g_{11}	12	$g_{12} = g_{21}$	-6
g_{22}	4	$k_{12} = k_{21}$	-1/10
k_{11}	6/5	$q_{12} = q_{21}$	1/1400
k_{22}	2/15	q_{11}	-1/700
q_{22}	-11/6300		

NOMENCLATURE

E	Young's Modulus, N/m^2.
Fo	Transverse load applied to primary mass, N.
Fo_x	Transverse load on beam x, N.
FRo_x	Reaction force on beam x acting along. the transverse direction, N.
g	Acceleration due to gravity, m/s^2.
I	Area moment of inertia of the flexible link, m^4.
L	Length of the beam, m.
L_i	Length of the inner beam, m.
L_o	Length of the outer beam, m.
ms_1	Intermediate mass, kg.
ms_2	Primary mass, kg.
Mo	Moment applied to primary mass, N.
Mo_x	Moment on beam x, N.
MRo_x	Reaction moment on beam x, Nm.
Po	Constant gravitational load acting on primary. mass along the axial direction, N.
Po_x	Axial load on beam x, N.
PRo_x	Reaction force on beam x acting along the. axial direction, N.
S_e	Endurance strength of beam material, N/m^2.
$stroke$	Maximum transverse displacement on one side. from mean position, m.
t_i	Thickness of the inner beam, m.
t_{max}	Maximum allowable beam thickness, m.
t_o	Thickness of the outer beam, m.
W_d	Difference between width of inner and outer. beam at desired primary mass.
W_d^*	Difference between width of inner and outer. beam when primary mass is 1 kg.
W_i	Width of the inner beam, m.
W_o	Width of the outer beam, m.
x	Suffix x indicates the beam number. throughout nomenclature.
Xo_x	Deformed length of beam x along axial. direction (see Fig. 26 in Appendix A), m.
Yo_x	Transverse deformation of beam x, m.
σ_{max}	Maximum normal stress, N/m^2.
θo_x	Slope at the end of beam x.

APPENDIX A
SUPPLEMENTARY FIGURES AND TABLES

See Figure 25–31 and Tables 3–5.

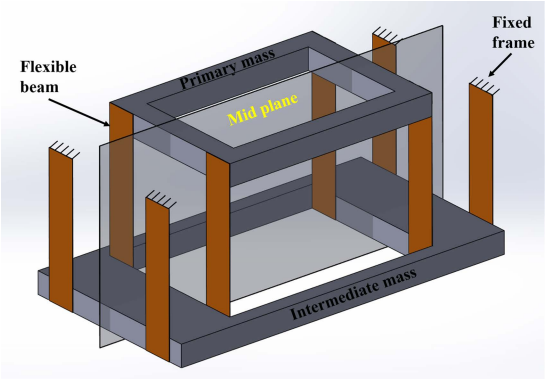

FIGURE 25. DPCM with 8 beams.

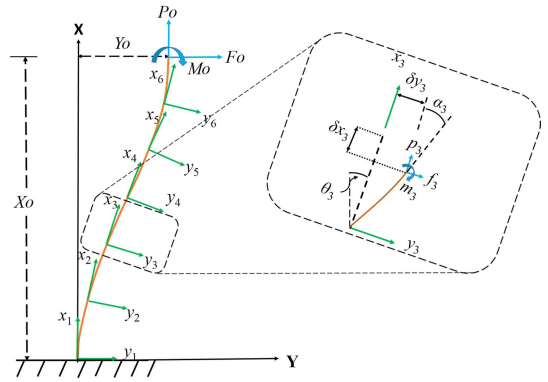

FIGURE 26. Flexible beam discretized into six elements [31].

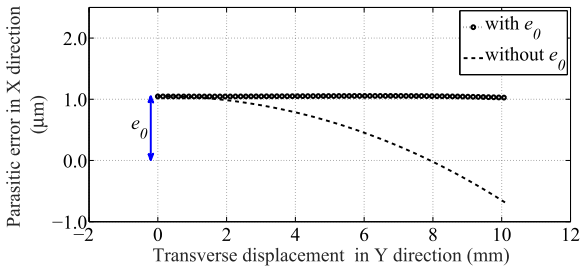

FIGURE 27. Trajectory of motion stage.

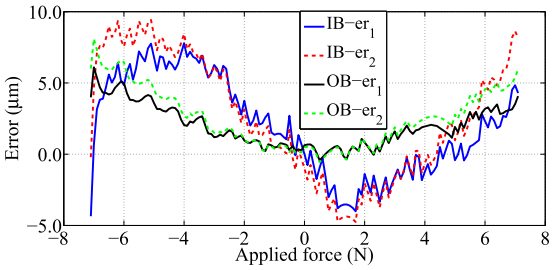

FIGURE 28. Error between experimental and simulation parasitic error for unoptimized DPCM: er_1: FEA and Experiment er_2: CBCM and Experiment.

APPENDIX B
ILLUSTRATIVE EXAMPLE FOR THE PROPOSED DESIGN PROCEDURE

The mass of rigid elements ms_1 and ms_2 of DPCM operating in orientation B is 8 kg and 10 kg respectively. The desired

TABLE 4. Equations to calculate *NSD*.

$\frac{t}{L}$	$\frac{ms_1}{ms_2}$	*Equation*
0.005	0.4	$NSD = -0.02308 \times \left(\frac{stroke}{L}\right)^3 + 0.001416 \times \left(\frac{stroke}{L}\right)^2 + 0.7292 \times \left(\frac{stroke}{L}\right) + 3.986e^{-06}$
	0.8	$NSD = -0.03118 \times \left(\frac{stroke}{L}\right)^3 + 0.001459 \times \left(\frac{stroke}{L}\right)^2 + 0.8504 \times \left(\frac{stroke}{L}\right) + 4.369e^{-06}$
	1.2	$NSD = -0.03847 \times \left(\frac{stroke}{L}\right)^3 + 0.001105 \times \left(\frac{stroke}{L}\right)^2 + 0.9717 \times \left(\frac{stroke}{L}\right) + 2.835e^{-06}$
0.0075	0.4	$NSD = 0.0462 \times \left(\frac{stroke}{L}\right)^3 - 0.01267 \times \left(\frac{stroke}{L}\right)^2 + 0.9786 \times \left(\frac{stroke}{L}\right) + 5.644e^{-05}$
	0.8	$NSD = 0.05469 \times \left(\frac{stroke}{L}\right)^3 - 0.01313 \times \left(\frac{stroke}{L}\right)^2 + 0.8574 \times \left(\frac{stroke}{L}\right) + 5.798e^{-05}$
	1.2	$NSD = 0.0462 \times \left(\frac{stroke}{L}\right)^3 - 0.01267 \times \left(\frac{stroke}{L}\right)^2 + 0.9786 \times \left(\frac{stroke}{L}\right) + 5.644e^{-05}$
0.01	0.4	$NSD = 0.3083 \times \left(\frac{stroke}{L}\right)^3 - 0.09904 \times \left(\frac{stroke}{L}\right)^2 + 0.7624 \times \left(\frac{stroke}{L}\right) + 0.0002904$
	0.8	$NSD = 0.3066 \times \left(\frac{stroke}{L}\right)^3 - 0.102 \times \left(\frac{stroke}{L}\right)^2 + 0.8839 \times \left(\frac{stroke}{L}\right) + 0.0003202$
	1.2	$NSD = 0.2963 \times \left(\frac{stroke}{L}\right)^3 - 0.1004 \times \left(\frac{stroke}{L}\right)^2 + 1.005 \times \left(\frac{stroke}{L}\right) + 0.0003126$

TABLE 5. Equations to calculate W_d.

$\frac{t}{L}$	$\frac{ms_1}{ms_2}$	*Equation*
0.005	0.4	$\frac{W_d}{W_d^*} = -2.026e^{-05} \times (ms_2)^4 + 3.917e^{-04} \times (ms_2)^3 - 2.758e^{-03} \times (ms_2)^2 + 1.002 \times (ms_2) - 1.293e^{-15}$
	0.8	$\frac{W_d}{W_d^*} = -2.947e^{-05} \times (ms_2)^4 + 4.614e^{-04} \times (ms_2)^3 - 2.801e^{-03} \times (ms_2)^2 + 1.002 \times (ms_2) - 1.315e^{-15}$
	1.2	$\frac{W_d}{W_d^*} = -8.718e^{-05} \times (ms_2)^4 + 1.104e^{-04} \times (ms_2)^3 - 4.743e^{-03} \times (ms_2)^2 + 1.004 \times (ms_2) - 1.449e^{-15}$
0.0075	0.4	$\frac{W_d}{W_d^*} = -3.335e-05 \times (ms_2)^4 + 0.0007134 \times (ms_2)^3 - 0.005189 \times (ms_2)^2 + 1.005 \times (ms_2) - 1.313e^{-15}$
	0.8	$\frac{W_d}{W_d^*} = -3.084e-05 \times (ms_2)^4 + 0.000629 \times (ms_2)^3 - 0.004541 \times (ms_2)^2 + 1.004 \times (ms_2) - 1.309e^{-15}$
	1.2	$\frac{W_d}{W_d^*} = -3.317e-05 \times (ms_2)^4 + 0.00061 \times (ms_2)^3 - 0.004209 \times (ms_2)^2 + 1.004 \times (ms_2) - 1.316e^{-15}$
0.01	0.4	$\frac{W_d}{W_d^*} = -0.000112 \times (ms_2)^4 + 0.002462 \times (ms_2)^3 - 0.01782 \times (ms_2)^2 + 1.015 \times (ms_2) - 1.443e^{-15}$
	0.8	$\frac{W_d}{W_d^*} = -0.0001479 \times (ms_2)^4 + 0.003198 \times (ms_2)^3 - 0.02244 \times (ms_2)^2 + 1.019 \times (ms_2) - 1.511e^{-15}$
	1.2	$\frac{W_d}{W_d^*} = -8.483e-05 \times (ms_2)^4 + 0.001862 \times (ms_2)^3 - 0.01352 \times (ms_2)^2 + 1.012 * (ms_2) - 1.397e^{-15}$

range of motion is 120 mm. The beam material has an elastic modulus of 100 Gpa and endurance strength is 500 Mpa. Find out the beam dimensions for which parasitic error of DPCM will be within 5 micron?

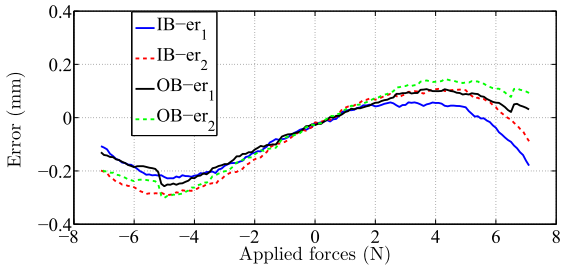

FIGURE 29. Error between experimental and simulation transverse displacement for unoptimized DPCM: er_1: FEA and Experiment er_2: CBCM and Experiment.

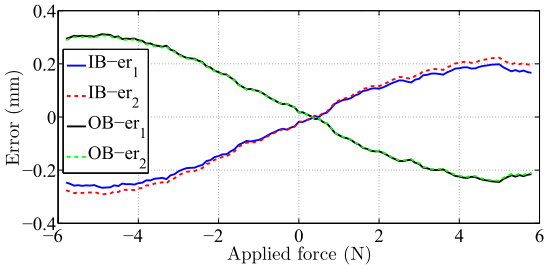

FIGURE 30. Error between experimental and simulation transverse displacement for optimized DPCM: er_1: FEA and Experiment er_2: CBCM and Experiment.

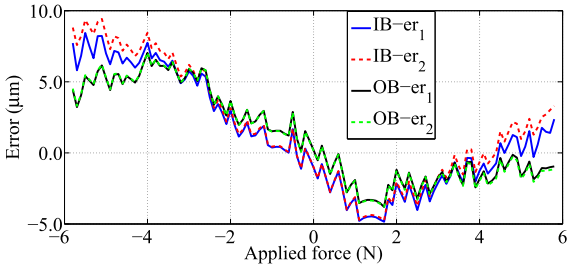

FIGURE 31. Error between experimental and simulation parasitic error for optimized DPCM: er_1: FEA and Experiment er_2: CBCM and Experiment.

Step 1: The inputs given in the problem for DPCM are

$$ms_1 = 8 \text{ kg}, \quad \text{and } ms_2 = 10 \text{ kg},$$
$$stroke = 60 \text{ mm}$$
(maximum motion on one side from mean position).

Now, length of the beam is selected such that the stroke is in between 1 to 40 % of the length of the beam. Therefore, $L = 200$ mm.

Step 2: Find maximum thickness (t_{max}) of the beam for the selected length ($L = 200$ mm) to avoid fatigue failure under the desired stroke using (13) as below

$$t_{max} = \frac{2L^2 S_e}{3Estroke} = \frac{2 \times (0.200)^2 \times 500 \times 10^6}{3 \times (100 \times 10^9) \times 0.060},$$
$$t_{max} = 0.0022 \text{ m} = 2.2 \text{ mm}.$$

We selected $t = 1.5$ mm such that $t < t_{max}$.

Step 3: For $\frac{t}{L} = 0.0075$, $\frac{stroke}{L} = 0.3$ and $\frac{ms_1}{ms_2} = 0.8$, we get $NSD = 0.2576$ from Fig. 17 shown in the Section IV-A4. Thus,

$$W_d^* = \frac{NSD.ms_2 gL^3}{Et^3.stroke} = \frac{0.2576 \times 1 \times 9.81 \times (0.200)^3}{(100 \times 10^9) \times 0.0015^3 \times 0.06},$$
$$W_d^* = 0.000998343 \text{ m} = 0.998343 \text{ mm}.$$

Step 4: From Fig. 18(b) of Section IV-A4, the value of $\frac{W_d}{W_d^*}$ is 9.906 at the desired primary mass of 10 kg. Therefore,

$$W_d = W_d^* \times 9.906 = 0.998343 \times 9.906$$
$$W_d = 9.88958 \text{ mm}.$$

Step 5: Find out $(W_i)_{min}$ to avoid buckling of inner beams from (15) as below

$$(W_i)_{min} = \frac{3ms_2 gL^2}{\pi^2 Et^3} = \frac{3 \times 10 \times 9.81 \times (0.200)^2}{\Pi^2 \times (100 \times 10^9) \times 0.0015^3},$$
$$(W_i)_{min} = 0.003534 \text{ m} = 3.5340 \text{ mm}.$$

We selected $W_i = 50$ mm such that $W_i > (W_i)_{min}$. Therefore $W_0 = 50 - 9.88958 = 40.1104$ mm. The dimensions of flexible beams obtained from the design steps for the considered example of DPCM are validated with CBCM.

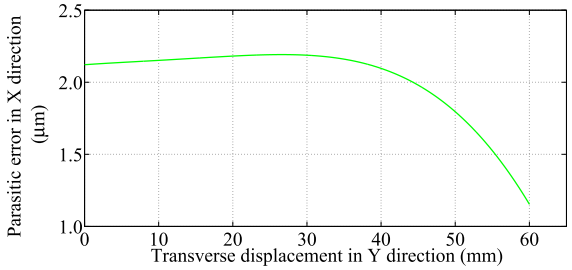

FIGURE 32. Path followed by motion stage.

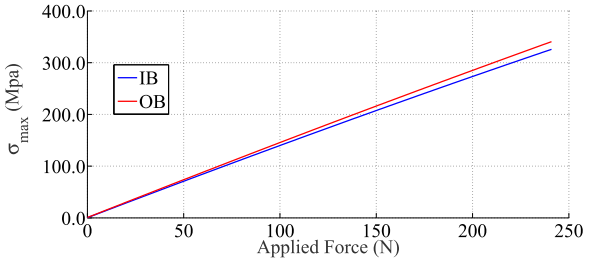

FIGURE 33. Stresses generated in inner and outer flexible beam.

Fig. 32 and 33 show that the parasitic error is within 1 micron over the stroke of 60 mm and maximum stresses induced during the desired stroke are less than the endurance strength, respectively.

APPENDIX C
LOAD EQUILLIBRIUM EQUATIONS FOR DPCM OPERATING IN ORIENTATION C

Load equilibrium equations of primary mass ms_2 are

$$Fo - Fo_1 - Fo_2 - ms_2 g = 0,$$

$$Po_1 + Po_2 = 0,$$
$$(Fo_1 + Fo_2)a + Po_1\left(\frac{b}{2}\right) = Po_2\left(\frac{b}{2}\right) + Mo_1 + Mo_2. \quad \text{(C16)}$$

Similarly, load equilibrium equations of intermediate mass ms_1 are

$$\begin{aligned} Fo_3 + Fo_4 + ms_1 g &= FRo_1 + FRo_2, \\ PRo_1 + PRo_2 &= -Po_3 - Po_4, \\ PRo_1\left(\frac{b}{2}\right) + Po_4\left(\frac{d}{2}\right) &= PRo_2\left(\frac{b}{2}\right) + Po_3\left(\frac{d}{2}\right) \\ &\quad -(Fo_3 + Fo_4)c + MRo_1 \\ &\quad +(FRo_1 + FRo_2)c + MRo_2 \\ &\quad +Mo_3 + Mo_4. \end{aligned} \quad \text{(C17)}$$

ACKNOWLEDGMENT

The authors would like to thank Raj Mashruwala for his financial support for the Development of Suman Mashruwala Advanced Micro Engineering Laboratory, IIT Bombay, where this work was carried out.

REFERENCES

[1] L. Howell, *Compliant Mechanisms*. New York, NY, USA: Wiley, 2002.
[2] E. Pernette, S. Henein, I. Magnani, and R. Clavel, "Design of parallel robots in microrobotics," *Robotica*, vol. 15, no. 4, pp. 417–420, Jul. 1997.
[3] H.-H. Pham, H.-C. Yeh, and I.-M. Chen, "Micromanipulation system design based on selective actuation mechanisms," *Int. J. Robot. Res.*, vol. 25, no. 2, pp. 171–186, Feb. 2006.
[4] A. Eisinberg, A. Menciassi, S. Micera, D. Campolo, M. C. Carrozza, and P. Dario, "PI force control of a microgripper for assembling biomedical microdevices," *IEE Proc. Circuits, Devices Syst.*, vol. 148, no. 6, pp. 348–352, Dec. 2001.
[5] S. E. Alper, K. M. Silay, and T. Akin, "A low-cost rate-grade nickel microgyroscope," *Sens. Actuators A, Phys.*, vol. 132, no. 1, pp. 171–181, Nov. 2006.
[6] H. Liu, W. Su, and F. Zhang, "A resonant accelerometer based on electrostatic stiffness and its closed-loop control method," *Sensor Rev.*, vol. 31, no. 1, pp. 58–64, Jan. 2011.
[7] Y.-M. Moon, "Bio-mimetic design of finger mechanism with contact aided compliant mechanism," *Mechanism Mach. Theory*, vol. 42, no. 5, pp. 600–611, May 2007.
[8] J.-M. Huang, A. Q. Liu, Z. L. Deng, Q. X. Zhang, J. Ahn, and A. Asundi, "An approach to the coupling effect between torsion and bending for electrostatic torsional micromirrors," *Sens. Actuators A, Phys.*, vol. 115, no. 1, pp. 159–167, Sep. 2004.
[9] S. Deshmukh and P. S. Gandhi, "Optomechanical scanning systems for microstereolithography (MSL): Analysis and experimental verification," *J. Mater. Process. Technol.*, vol. 209, no. 3, pp. 1275–1285, Feb. 2009.
[10] T. U. Islam and P. S. Gandhi, "Fabrication of multscale fractal-like structures by controlling fluid interface instability," *Sci. Rep.*, vol. 6, no. 1, Dec. 2016, Art. no. 37187.
[11] M. J. Van de Moosdijk, E. Van den Brink, K. Simon, A. Friz, G. N. Phillipps, R. J. Travers, and E. Raaymakers, "Collinearity and stitching performance on an ASML stepper," in *Proc. Emerg. Lithographic Technol. VI*, Jul. 2002, pp. 858–866.
[12] X. M. Zhang, F. S. Chau, C. Quan, Y. L. Lam, and A. Q. Liu, "A study of the static characteristics of a torsional micromirror," *Sens. Actuators A, Phys.*, vol. 90, nos. 1–2, pp. 73–81, 2001.
[13] G. Dai, F. Pohlenz, H.-U. Danzebrink, M. Xu, K. Hasche, and G. Wilkening, "Metrological large range scanning probe microscope," *Rev. Sci. Instrum.*, vol. 75, no. 4, pp. 962–969, 2004.
[14] L.-J. Lai, G.-Y. Gu, and L.-M. Zhu, "Design and control of a decoupled two degree of freedom translational parallel micro-positioning stage," *Rev. Sci. Instrum.*, vol. 83, no. 4, Apr. 2012, Art. no. 045105.
[15] S. Lin, Y. Jia, I. P. Lei, and Q. Xu, "Design and optimization of a long-stroke compliant micropositioning stage driven by voice coil motor," in *Proc. 12th Int. Conf. Control Autom. Robot. Vis. (ICARCV)*, Dec. 2012, pp. 1716–1721.
[16] X. Sun, W. Chen, R. Zhou, J. Zhang, and W. Chen, "Design of compliant parallel mechanism for nanoimprint lithography," in *Proc. 6th IEEE Conf. Ind. Electron. Appl.*, Jun. 2011, pp. 200–205.
[17] Q. Xu, "A novel compliant micropositioning stage with dual ranges and resolutions," *Sens. Actuators A, Phys.*, vol. 205, pp. 6–14, Jan. 2014.
[18] H. Zhao, D. Han, L. Zhang, and S. Bi, "Design of a stiffness-adjustable compliant linear-motion mechanism," *Precis. Eng.*, vol. 48, pp. 305–314, Apr. 2017.
[19] L. Rubbert, R. Bitterli, N. Ferrier, S. Fifanski, I. Vardi, and S. Henein, "Isotropic springs based on parallel flexure stages," *Precis. Eng.*, vol. 43, pp. 132–145, Jan. 2016.
[20] G. Hao, H. Li, X. He, and X. Kong, "Conceptual design of compliant translational joints for high-precision applications," *Frontiers Mech. Eng.*, vol. 9, no. 4, pp. 331–343, Dec. 2014.
[21] R. M. Panas and J. B. Hopkins, "Eliminating underconstraint in double parallelogram flexure mechanisms," *J. Mech. Des.*, vol. 137, no. 9, Sep. 2015, Art. no. 092301.
[22] R. Frisch-Fay, *Flexible Bars*. Washington, DC, USA: Butterworth, 1962.
[23] O. A. Turkkan and H.-J. Su, "A general and efficient multiple segment method for Kinetostatic analysis of planar compliant mechanisms," *Mechanism Mach. Theory*, vol. 112, pp. 205–217, Jun. 2017.
[24] M. Niu, B. Yang, Y. Yang, and G. Meng, "Two generalized models for planar compliant mechanisms based on tree structure method," *Precis. Eng.*, vol. 51, pp. 137–144, Jan. 2018.
[25] M. Ling, J. Cao, and N. Pehrson, "Kinetostatic and dynamic analyses of planar compliant mechanisms via a two-port dynamic stiffness model," *Precis. Eng.*, vol. 57, pp. 149–161, May 2019.
[26] F. Ma and G. Chen, "Modeling large planar deflections of flexible beams in compliant mechanisms using chained beam-constraint-model1," *J. Mech. Robot.*, vol. 8, no. 2, Apr. 2016, Art. no. 021018.
[27] S. Awtar, A. H. Slocum, and E. Sevincer, "Characteristics of beam-based flexure modules," *J. Mech. Des.*, vol. 129, no. 6, pp. 625–639, May 2007.
[28] R. Bafna, A. Tanksale, and P. Gandhi, "Fabrication of micro-compliant mechanisms using micro-stereolithography," in *Mechanism and Machine Science*, D. Sen, S. Mohan, and G. K. Ananthasuresh, Eds. Singapore: Springer, 2021, pp. 547–555.
[29] X. Pei, J. Yu, G. Zong, and S. Bi, "Design of compliant straight-line mechanisms using flexural joints," *Chin. J. Mech. Eng.*, vol. 27, no. 1, pp. 146–153, Jan. 2014.
[30] A. H. Slocum, *Precision Machine Design*. Southfield, MI, USA: Society of Manufacturing Engineers, 1992.
[31] A. A. Tanksale and P. S. Gandhi, "Large deformation analysis and experiments with double parallelogram compliant mechanisms," in *Proc. ASME Int. Mech. Eng. Congr. Expo.*, 2018, Art. no. V04AT06A024.
[32] S. Awtar and S. Sen, "A generalized constraint model for two-dimensional beam flexures: Nonlinear load-displacement formulation," *J. Mech. Des.*, vol. 132, no. 8, pp. 345–358, Aug. 2010.
[33] P. Gandhi, K. Sonawale, V. Soni, N. Patanwala, and A. Bansode, "Design for assembly guidelines for high-performance compliant mechanisms," *J. Mech. Des.*, vol. 134, no. 12, Dec. 2012, Art. no. 121006.

TANKSALE ABHIJIT is currently pursuing the Ph.D. degree with the Mechanical Engineering Department, Indian Institute of Technology Bombay, Mumbai, India. His research interests include theoretical and experimental analysis of compliant mechanisms with large deformation.

GANDHI PRASANNA (Member, IEEE) received the Ph.D. degree from Rice University, Houston, TX, USA, in 2001. He is currently a Professor with the Indian Institute of Technology Bombay, Mumbai, India. His research interests include robotics, mechatronics, multi-scale manufacturing using fluid instabilities, 3D micro printing, and dynamic systems and controls.